Structural and Motional Changes Induced in *apo*-S100A1 Protein by the Disulfide Formation between Its Cys 85 Residue and β-Mercaptoethanol[†,‡]

Igor Zhukov,[§,||] Andrzej Ejchart,[§] and Andrzej Bierzyński*[,§]

Institute of Biochemistry and Biophysics, Polish Academy of Sciences, Pawińskiego 5A, 02-106 Warsaw, Poland, and Slovenian NMR Centre, National Institute of Chemistry, Hajdrihova 19, P.O.B. 660, SI-1001 Ljubljana, Slovenia

Received September 4, 2007; Revised Manuscript Received October 26, 2007

ABSTRACT: Recently, we have shown (Goch, G., Vdovenko, S., Kozłowska, H., and Bierzyński, A. (2005) *FEBS J. 272*, 2557−2565) that the chemical modification of Cys 85 residue of S100A1 protein by disulfide bond formation with small thiols such as glutathione, cysteine, or β-mercaptoethanol (βME) leads to a dramatic increase of the protein affinity for calcium. Therefore, the biological function of S100A1 as a calcium signal transmitter is probably regulated by the redox potential within the cell. Systematic, structural studies of various mixed disulfides of S100A1 in the *apo* and *holo* states are necessary to elucidate the mechanism of this phenomenon. Using NMR methods we have determined the structure of *apo*-S100A1-βME and, on the basis of ^{15}N nuclear magnetic relaxation data, we have characterized the structural dynamics of both: modified and unmodified molecules of *apo*-S100A1. The following effects of βME modification have been observed: (1) Helices IV and IV′ of two protein subunits are elongated by five residues (85−89). (2) Conformation of the calcium binding N-terminal loops is dramatically changed, and structural flexibility of the N-loops as well as C-loops markedly increases. (3) The angle between helices I and IV increases by ∼20° and between helices IV and IV′ decreases by ∼35°. All these observations lead to the conclusion that βME modification of *apo*-S100A1 makes its structure more similar to that of *holo*-S100A1, so that it becomes much better adjusted for calcium coordination.

Calcium ion is one of the most important messengers regulating numerous vital biological processes. A crucial role in the calcium signal transduction is played by EF-hand proteins that coordinate calcium and change their conformation exposing hydrophobic patches to which a large variety of target proteins bind.

S100 is a subfamily of EF-hand proteins found only in mammals and avians, implicated in cell growth, motility, and cell differentiation, by a variety of processes such as regulation of some enzyme as well as transcription factor activities, Ca^{2+} homeostasis, and regulation of cytoskeleton dynamics. Some of them have extracellular cytokine-like activities (*1*, *2*). Recently, S100 proteins have received increasing attention due to their close association with several human diseases including cardiomyopathy, neurodegenerative disorders, and cancer (*2*).

S100A1 protein, intensively studied since its discovery in 1965 (*3*), is, in every respect, a typical representative of the S100 family. The structure of S100A1 in the *apo* state has been determined by Rustandi et al. (*4*) using NMR methods. Recently, its structure in the *holo* state has also been solved (*5*). The protein molecule is a symmetrical homodimer, strongly stabilized by hydrophobic interactions between its two α subunits. Each subunit contains two EF-hand motives that coordinate calcium ions in a noncooperative way with the binding constants, at physiological pH (7.2) and NaCl concentration (100 mM), of the order of 10^3 M^{-1} for C-terminal motives and 10^2 M^{-1} for N-terminal ones (*6*).

These values are too low for a calcium-signaling protein, because the intracellular calcium concentration of Ca^{2+} ions never exceeds ≈1 μM, even during the calcium stress (*7*). We have found, though, that the formation of a mixed disulfide between glutathione, cysteine, or β-mercaptoethanol (βME)[1] and the single cysteine residue present in position 85 in both protein subunits leads to a dramatic increase of S100A1 affinity for calcium (*6*). This observation suggests that the calcium-dependent biological activity of the protein can be regulated by thionylation, most probably glutathionylation, because of high concentration of glutathione in the cell (∼10 mM). Therefore, S100A1 can play the role of a linker between the two most important signaling pathways, i.e., the redox- and calcium-dependent ones.

What is the structural mechanism responsible for this phenomenon? To answer this question it is necessary to compare the structures of S100A1 and its mixed disulfides

[†] This work was supported by Polish Committee for Scientific Research Grant 6 P04 009 16.

[‡] The coordinates have been deposited in the Protein Data Bank (code 2JPT).

* To whom correspondence should be addressed. Telephone: (48 22) 592-23-71. Fax: (48 22) 823-71-94. E-mail: ajb@ibb.waw.pl.

[§] Polish Academy of Sciences.

[||] National Institute of Chemistry.

[1] Abbreviations: βME, β-mercaptoethanol; DSS-d_4, 3-trimethylsilyl-2,2,3,3-tetradeuteropropionic acid sodium salt; EDTA, ethylenediaminetetraacetic acid; HSQC, heteronuclear single quantum coherence; HPLC, high performance liquid chromatography; NMR, nuclear magnetic resonance; NOE, nuclear Overhauser effect; S100A1-βME, mixed disulfide of *apo*-S100A1 protein with β-mercaptoethanol; TRIS-d_{11}, perdeuterated 2-amino-2-(hydroxymethyl)1,3-propanediol.

10.1021/bi701762v CCC: $40.75
Published on Web 12/19/2007

in the *apo* and *holo* states. Valuable information can also be obtained from comparative studies of the structural dynamics of these molecules. In particular, comparative studies of the protein modified with glutathione and βME, the substituents so different chemically, yet similarly enhancing the protein calcium-binding ability, is interesting, making it possible to discern between relevant and nonrelevant conformational changes induced by a substituent.

In this paper we present the NMR structure of *apo*-S100A1 modified by βME and compare it with the structure of the unmodified protein determined by Rustandi et al. (*4*). Structural flexibilities of both molecules, as determined by nuclear magnetic relaxation methods, are also compared.

MATERIALS AND METHODS

Sample Preparation. ^{15}N-labeled and ^{13}C,^{15}N-double labeled S100A1 protein was expressed as previously described (*8*). Shortly: The synthetic gene coding for bovine S100α subunit with the amino acid sequence determined by Isobe and Okuyama (*9*) was cloned into a derivative of pAED4 plasmid and expressed in *Escherichia coli* utilizing the T7 expression system. The bacteria were grown in M9 medium containing $(^{15}NH_4)_2SO_4$ as the sole nitrogen source and either unlabeled or ^{13}C-labeled glucose as the sole carbon source.

The expression products were isolated using a phenyl-sepharose column, purified by reverse-phase HPLC on a semipreparative Vydac C18 column, and identified by the electrospray ionization mass spectrometry using a Macromass Q-Tof spectrometer (*6*). Because 1 mM concentration of β-mercaptoethanol was maintained during *E. coli* cell sonification and isolation of the recombinant protein, its disulfide with β-mercaptoethanol (S100A1-βME) predominates in preparations and can be easily separated by HPLC from the reduced S100A1 molecules.

Two forms of the protein, (a) with the sequence strictly corresponding to its gene sequence and (b) with the additional initiator methionine at the N-terminus, come from HPLC as partly overlapping peaks. NMR measurements indicated that structural differences between both forms are small and localized to the close vicinity of the N-terminal Met residue (*10*). Therefore, a mixture of (a) and (b) species was used in all experiments.

600 μL NMR samples contained 1.1 mM protein solution (monomer concentration) in 90%/10% H_2O/D_2O, 50 mM TRIS-d_{11}, 2.9 mM EDTA, 0.1 mM NaN_3, and 96 mM $KClO_4$ with pH adjusted to 6.3 (uncorrected value). For ^{13}C,^{15}N-double labeled protein the sample volume was limited to 250 μL and NMR measurements were performed using a Shigemi tube.

NMR Spectroscopy. NMR measurements were performed on Varian Inova 400 MHz (9.4 T), Varian Unity+ 500 MHz (11.7 T), and Varian Inova 750 MHz (17.6 T) spectrometers at 35 °C carefully adjusted with ethylene glycol reference sample. All spectrometers were equipped at least with three channels, a *z*-axis pulsed field gradient unit, and a triple {^{13}C,^{15}N}^{1}H probe with gradient coil(s) and the inverse detection. All heteronuclear NMR data were acquired using the States-TPPI quadrature detection (*11*) followed by the sensitivity enhanced detection introduced by Kay et al. (*12*). 1.4 s recycling delay was used, if not stated otherwise. All chemical shifts in heteronuclear NMR spectra were reported with respect to external DSS-d_4. Chemical shifts of ^{13}C and ^{15}N signals were referenced indirectly using the following ratios of the zero-point frequencies: $f(^{13}C)/f(^1H) = 0.251449530$ and $f(^{15}N)/f(^1H) = 0.101329118$ (*13*). Experimental data were processed using the NMRPipe software package (*14*). The processed spectra were analyzed with both the XEASY (*15*) and SPARKY (*16*) software.

Table 1: Parameters of NMR Experiments Used for the Structure Determination of *apo*-S100A1-βME Protein[a]

experiment	dim	nucl	time pts	acq time (ms)
2D [^{1}H−^{15}N]HSQC	t_1	^{15}N	64	49.2
	t_2	^{1}H	512	83.9
3D HNHA (17.6 T)	t_1	^{1}H	64	12.8
	t_2	^{15}N	16	16.0
	t_3	^{1}H	512	83.9
3D ^{15}N-edited NOESY-HSQC (17.6 T), 150 ms mixing time	t_1	^{1}H	320	35.5
	t_2	^{15}N	24	19.3
	t_3	^{1}H	720	80.0
3D HNCO, 3D C(CO)NH, 3D (HCA)CO(CA)NH, 3D H(CCO)NH	t_1	^{13}C	32	16.8
	t_2	^{15}N	16	12.3
	t_3	^{1}H	384	62.9
3D HN(CO)CA, 3D HNCA, 3D CBCA(CO)NH, 3D HNCACB	t_1	^{13}C	32	9.4
	t_2	^{15}N	16	12.3
	t_3	^{1}H	384	62.9
3D ^{13}C-edited NOESY-HSCQ, (17.6 T), 100 ms mixing time	t_1	^{1}H	320	35.5
	t_2	^{13}C	24	19.3
	t_3	^{1}H	720	80.0

[a] If not indicated otherwise, experiments were carried out at 11.7 T. Zero filling in all dimensions was applied prior to the Fourier transformation.

The sequence-specific assignment was performed on the uniformly ^{13}C,^{15}N-double labeled sample of *apo*-S100A1-βME. The 3D heteronuclear HNCACB (*17*), CBCA(CO)NH (*18*), HNCA (*19*), HN(CO)CA (*20*), HNCO (*21*), (HCA)CO(CA)NH (*22*) spectra were used to obtain assignments of backbone ^{1}H, ^{13}C, and ^{15}N resonances using standard methods (*21*). Aliphatic side chain ^{1}H and ^{13}C resonances were assigned from the analysis of the heteronuclear 3D C(CO)NH and H(CCO)NH (*23*), and 2D [^{1}H-^{13}C] HSQC spectra. Aromatic side chain resonances were assigned from the ^{13}C-edited NOESY-HSQC spectrum recorded with the offset, spectral widths, and ^{13}C−^{1}H coupling constants tuned to aromatic carbons. 74 backbone scalar coupling constants $^3J(H_N,H_\alpha)$ were determined using the HNHA experiment.

The detailed information about all experiments is collected in Table 1. ^{1}H, ^{13}C, and ^{15}N chemical shifts were deposited in the BMRB database (http://www.bmrb.wisc.edu) under the accession number 4982.

Assignments of H_N, N, C′, C_α, and C_β chemical shifts in *apo*-S100A1 were performed using the same techniques as in the case of *apo*-S100A1-βME protein.

Relaxation experiments were performed at two magnetic fields, 9.4 and 11.7 T, on ^{15}N-labeled samples of either *apo*-S100A1 or *apo*-S100A1-βME protein. Longitudinal (R_1) and transverse (R_2) relaxation rates were measured using a sensitivity enhanced [^{15}N−^{1}H] HSQC pulse sequence (*12*) with the option of either R_1 or R_2 measurements of ^{15}N nuclei (*24*). Each spectrum was acquired with 512 (t_2) × 128 (t_1)

complex data points and the sweep widths of 6000 Hz in ^{1}H and 1300 Hz in ^{15}N dimensions. Zero filling was performed prior to the Fourier transformation. In the case of R_1 eleven relaxation delays of 10, 30, 90, 130, 210, 290, 370, 490, 610, 730, and 850 ms were used. The R_2 relaxation rate measurements were performed with the Carr−Purcell−Meiboom−Gill (CPMG) pulse train. Refocusing time of 650 μs was used during the relaxation delays which were set to 10, 30, 50, 70, 90, 130, 170, 210, and 250 ms. The acquisition parameters for R_1 and R_2 measurements were identical with the exception of the delay between π (^{1}H) pulses used for the cross-correlation effect suppression (*25*). 5 and 10 ms delays were used in R_1 and R_2 measurements, respectively. Delay between the scans of 1.8 s was employed in both experiments. {^{1}H}−^{15}N NOEs were measured with the pulse sequence included in the ProteinPack Varian Inc. (Palo Alto, CA) software. To increase its accuracy the dynamic variant of the experiment was chosen (*26*). The ^{1}H saturation time was set to 0.1, 0.15, 0.3, 0.7, 1.3, and 2.1 s. 32 scans per t_1 increment and the recycling delay of 3.2 s were employed. In all relaxation measurements the ^{15}N decoupling during the acquisition was applied using the GARP sequence with $\gamma B_2/2\pi = 3200$ Hz (*27*). All spectra were processed using the NMRPipe (*14*) and analyzed with the XEASY (*15*) programs.

Structure Calculations. The cross-peak assignment in NOESY spectra of S100 proteins is seriously complicated by poor resonance dispersion owing to a high content of the α-helical secondary structure and by the ambiguity arising from the symmetrical, dimeric structure of their molecules. Nevertheless, the cross-peak dispersion in the ^{1}H/^{15}N-HSQC spectrum of S100A1-βME protein was fairly good (Figure 1), much better than in the case of *apo*-S100A1. Therefore, the ^{15}N-edited NOESY-HSQC and ^{13}C-edited NOESY-HSQC spectra of S100A1-βME performed at high magnetic field strength (17.6 T) were informative enough to assign unequivocally intersubunit constraints among protons situated on the subunit interface of the protein (helices I, I′, IV, and IV′), so that measurements of 4D spectra were not necessary, although they had been indispensable for structure determination of *apo*- as well as *holo*-S100A1 protein (*4*, *5*).

Strong (1.8−2.9 Å), medium (1.8−3.5 Å), weak (1.8−4.5 Å), and very weak (1.8−5.5 Å) intrasubunit as well as intersubunit distance constraints were assigned from cross-peaks in the heteronuclear 3D ^{15}N-edited NOESY-HSQC (150 ms mixing time) and ^{13}C-edited NOESY-HSQC (100 ms mixing time) spectra. The pseudo-atom corrections were applied to the upper limits of constraints for methyl, methylene, and aromatic ring protons (*28*). +0.3 Å correction was added to upper limits of distance constraints involving methyl groups to account for a higher intensity of methyl resonances (*29*).

In order to distinguish between intra- and intersubunit NOE-derived distance constraints, the protocol introduced by Nilges (*30*) was used, resulting in identification of 286 intersubunit constraints. Backbone dihedral constraints ($-80° < \varphi < -40°$ and $-55° < \psi < -25°$ for α-helices and $-160° < \varphi < -80°$ and $100° < \psi < 180°$ for β-strands) were included in the structure calculation on the basis of $^3J(H_N,H_\alpha)$ scalar coupling constants ($J < 5$ Hz for α-helices and $J > 8$ Hz for β-strands) (*28*). Additional constraints for φ and ψ backbone torsion angles were evaluated using the

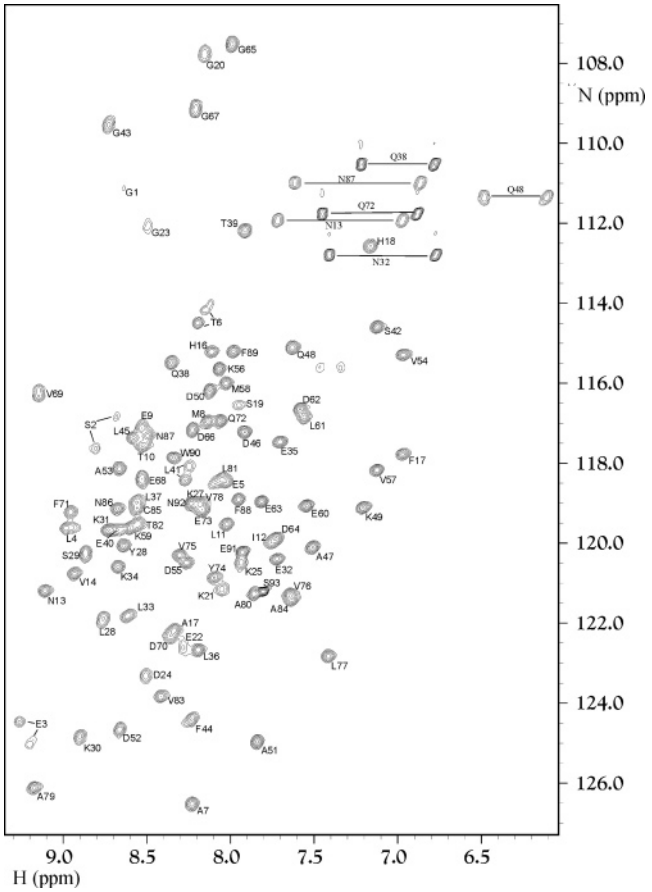

FIGURE 1: Amide correlations in the [^{15}N−^{1}H] HSQC spectrum of *apo*-S100A1-βME protein at 11.7 T. Pairs of side chain primary amide correlations in asparagines and glutamines are connected by horizontal solid lines.

TALOS software package (*31*). The predictions for 70 residues out of 93 were classified as "good" and used in the structure calculations after the fivefold increase of their deviations. 230 constraints for χ_1 and χ_2 torsion angles were evaluated by the GLOMSA and HABAS (gridsearch procedure) programs (*32*) included in the CYANA 1.0.6 software (*33*). The distance restraints ($r_{HN-O} = 1.5-2.8$ Å and $r_{N-O} = 2.4-3.5$ Å) for 72 backbone hydrogen bonds in regions of regular secondary structures (*28*) were included in the final stage of structure calculations. This procedure was the same as that applied previously by Wright et al. during the structure calculations of *holo*-S100A1 (*5*), which makes more trustworthy the comparisons between the structure solved by us and that of *holo*-S100A1 published by Wright et al. (PDB accession no. 1ZFS).

Determination of the spatial structure of *apo*-S100A1-βME was done using the XPLOR-NIH package based on the X-PLOR software (*34*), extended with the NMR-specific modules (*35*). Calculations started from a monomer template structure with randomly chosen φ and ψ torsion angles. In the first step, the structure was duplicated providing two identical, completely overlapping monomers. The standard calculation protocol included simulated annealing (12 ps at 3000 K) followed by slow cooling to 100 K combined with the final refinement procedure. The potential energy term for a noncrystallographic symmetry (NCS) was included in the simulated annealing procedure as described by Nilges (*30*).

The β-mercaptoethanol molecule was created using the standard molecular geometry and introduced as a hetero compound to the X-PLOR topology and parameter files (*34*). The generation of topology for *apo*-S100A1-βME protein was done by application of a specific patch to create the S−S bond between βME and Cys 85.

Analysis of ^{15}N Relaxation Data. All relaxation parameters (R_1, R_1, NOE) were determined by a two-parameter nonlinear least-squares fit of cross-peak heights to a single-exponential decay.

Two relaxation mechanisms have to be taken into account for the nuclear spin relaxation of amide nitrogens in proteins: the chemical shift anisotropy of a nitrogen nucleus and the dipole−dipole interaction between a nitrogen and the hydrogen directly bound to it. Equations describing relaxation parameters in terms of spectral density functions are given by (*36*)

$$R_1 = \frac{1}{4}D^2[J(\omega_H - \omega_N) + 3J(\omega_N) + 6J(\omega_H + \omega_N)] + \frac{1}{3}C^2J(\omega_N)$$

$$R_2 = \frac{1}{8}D^2[4J(0) + J(\omega_H - \omega_N) + 3J(\omega_N) + 6J(\omega_H) + 6J(\omega_H + \omega_N)] + \frac{1}{18}C^2[4J(0) + 3J(\omega_N)] + R_{ex}$$

$$\mathrm{NOE} = 1 + (\gamma_H/\gamma_N)\frac{D^2}{4R_1}[6J(\omega_H + \omega_N) - J(\omega_H - \omega_N)]$$

where $D = [\mu_0/(4\pi)][(\gamma_N\gamma_H\hbar)/\langle r_{NH}^3\rangle]$, $C = \omega_N\Delta\sigma$, and other symbols have their usual meaning. The values of $r_{NH} = 0.105$ nm and $\Delta\sigma = -160$ ppm (*36*) were used in calculations. The additional term R_{ex} takes into account the conformational exchange contribution to R_2 resulting from processes in the micro- to millisecond time scale often referred to as chemical exchange effects (*36*, *37*). Such processes, slower than the molecular tumbling, but fast enough to average chemical shifts, can influence transverse relaxation rates determined using the CPMG method. R_{ex} contribution to the transverse relaxation rate is proportional to the square of the chemical shift difference between exchanging states, $\Delta\delta$, and to ω_N, the Larmor frequency. It should be pointed out that the conformational exchange mechanism can affect the apparent transverse relaxation rate only if $\Delta\delta \neq 0$.

In the case of an isotropic molecular tumbling the model-free approach spectral density function takes the form (*38*)

$$J(\omega) = \frac{2}{5}[S^2\tau_R/[1 + (\omega\tau_R)^2] + (1 - S^2)\tau/[1 + (\omega\tau)^2]]$$

with $\tau^{-1} = \tau_R^{-1} + \tau_{int}^{-1}$. The isotropic overall motion is described by the correlation time τ_R and internal motion(s) by the generalized order parameter S, which is a measure of spatial restriction of the motion and of the effective correlation time τ_{int} describing the rate of this motion.

In the case of an anisotropic overall motion the spectral density function becomes more complex. Combining the model-free approach with an axially anisotropic overall tumbling (*39*), the spectral density function takes the form (*40*)

$$J(\omega) = \sum_k A_k(\alpha)\, J_{MFA}(S,\tau_{R,k},\tau_k;\omega)$$

where α is the angle between the N−H vector and the unique axis of the rotational diffusion tensor. Three coefficients $A_k(\alpha)$ have the form

$$A_1 = 0.75(\sin^4\alpha),$$
$$A_2 = 3(\sin^2\alpha)(\cos^2\alpha),$$
$$A_3 = 0.25(3\cos^2\alpha - 1)^2$$

and corresponding correlation times $\tau_{R,k}$ are defined as

$$\tau_{R,1} = 1/(4D_{||} + 2D_\perp),$$
$$\tau_{R,2} = 1/(D_{||} + 5D_\perp),$$
$$\tau_{R,3} = 1/(6D_\perp)$$

where $D_{||}$ and $D_\perp$ are the parallel and perpendicular components of the rotational diffusion tensor.

Table 2: Diffusion Tensor Parameters Obtained for *apo*-S100A1-βME and *apo*-S100A1 Proteins from a Model-Free Analysis Assuming the Axial Symmetry of the Diffusion Tensor

protein	*apo*-S100A1	*apo*-S100A1-βME
ratios of the principal values of moment of inertia	0.722:0.823:1.000	0.689:0.671:1.000
expected ratio of diffusion coefficients	0.965	0.950
experimental $D_{||}$	$(2.04 \pm 0.17) \times 10^7\ s^{-1}$	$(2.06 \pm 0.11) \times 10^7\ s^{-1}$
experimental $D_\perp$	$(2.31 \pm 0.14) \times 10^7\ s^{-1}$	$(2.14 \pm 0.09) \times 10^7\ s^{-1}$
experimental $D_{||}/D_\perp$	0.88 ± 0.09	0.96 ± 0.07
average τ_R[a]	7.51 ± 0.17 ns	7.89 ± 0.12 ns

[a] Calculated using the equation $\tau_R = (2D_{||} + 4D_\perp)^{-1}$.

Atomic coordinates of the NMR-derived structure of S100A1-βME were used to calculate the inertia tensor. The ratios of its principal values are given in Table 2 with the z-axis collinear with the symmetry axis of the homodimeric protein. For S100A1 protein the solution structure of rat *apo*-S100A1 was used (*4*) (PDB accession no. 1K2H) resulting in similar ratios of principal values of the inertia tensor (Table 2). Both structures were also used to calculate the geometric coefficients $A_k(\alpha)$. Because of the symmetry requirement it was assumed that rotational diffusion of both proteins is well represented by axially symmetric oblate tensors with their unique axis collinear with the protein symmetry axis.

The least-squares procedure used to optimize model parameters consisted of minimization through a grid-search of the target function χ^2 defined as follows:

$$\chi^2 = \sum_i\sum_j\sum_k (P_{ijk,ex} - P_{ijk,calc})^2/\sigma_{ijk}^2$$

where the sums are over the two magnetic fields used, the number of amino acid residues for which data are available (N), and the three relaxation parameters. The subscript ex refers to the experimentally obtained relaxation parameters and the subscript calc to the respective relaxation parameters

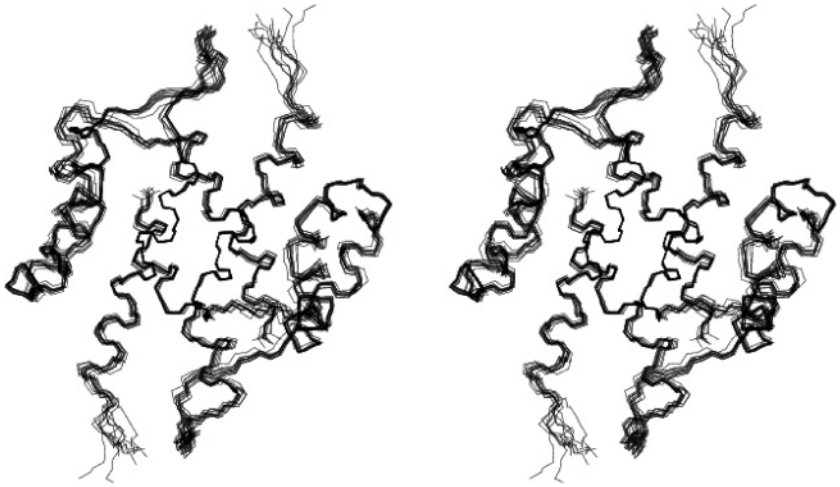

FIGURE 2: Stereoview of ten lowest total energy structures of *apo*-S100A1-βME protein.

calculated from the model. σ_{ijk} values are the standard deviations of the experimentally obtained parameters.

At this stage of the analysis the relaxation data for amino acid residues for which only the data at 11.7 T were available (Gly 23, Lys 27, Glu 40, Glu 73, Val 78) or the NOE values were distinctly small (Ser 2 at the N-terminus and Trp 90 through Ser 93 at the C-terminus) were excluded from the calculation. The minimization procedure delivered two global parameters $D_{||}$ and $D_{\perp}$ and N sets of local parameters S^2_j, τ_j, and $R_{ex,j}$. Uncertainties of the calculated parameter values were estimated as standard deviations from 200 Monte Carlo simulations.

Using the $D_{||}$ and $D_{\perp}$ values determined in this way, the local model-free parameters for 5 residues, previously omitted due to the lack of data obtained at two magnetic fields, were also calculated. On the other hand, the highly mobile terminal residues, Ser 2 and Trp 90 to Ser 93, cannot be regarded as a part of a rigid rotor, and description of their motions in terms of a single rotational diffusion tensor is not appropriate. In such a case the motion of an N−H vector in the *i*th residue should be described by the model-free approach spectral density functions in which the global parameter τ_R is substituted for a local one, $\tau_{R,i}$ (*41*, *42*).

RESULTS

Structure Determination of apo-S100A1-βME. Initial calculations based on distance constraints derived from the ^{15}N-edited NOESY-HSQC spectrum provided a medium resolution (~3.5 Å) three-dimensional structure of the *apo*-S100A1-βME protein. This initial structure was used in the further procedure of intersubunit/intrasubunit cross-peak discrimination in the 3D ^{13}C-edited NOESY-HSQC spectrum. Finally, 1098 intraresidual, 282 sequential, 398 medium range, 248 long range, and 286 intersubunit interproton distance constraints were included in the structure calculations.

The overlay of the 10 lowest energy structures of the protein is shown in Figure 2, and the structure calculation statistics is given in Table 3. None of these structures contain NOE violations exceeding 0.3 Å and dihedral angle violations larger than 5°. The analysis made using the PROCHECK-NMR program (*43*) indicates that the average structure is well-defined, corresponding to the X-ray resolution of 1.6 Å.

Table 3: NMR Constraints and Statistics of 10 NMR-Derived *apo*-S100A1-βME Structures with the Lowest Total Energy

	<10>	best
rmsd from distance constraints[a]		
total (2384)	0.0133 ± 0.0005	0.0126
intraresidual ($\|i$-$j\| = 0$) (1098)	0.0078 ± 0.0017	0.0066
sequential ($\|i - j\| = 1$) (282)	0.0182 ± 0.0019	0.0208
medium range ($\|i - j\| \leq 5$) (398)	0.0171 ± 0.0011	0.0163
long range ($\|i - j\| > 5$) (248)	0.0150 ± 0.0022	0.0131
intersubunits (286)	0.0152 ± 0.0031	0.0115
hydrogen bonds (72)	0.0130 ± 0.0026	0.0131
rmsd from dihedral angles constraints[a]		
total (558)	0.360 ± 0.040	0.348
backbone (φ/ψ) (328)	0.462 ± 0.057	0.449
side chain (χ_1/χ_2) (230)	0.101 ± 0.042	0.092
rmsd from idealized covalent geometry		
bonds (Å)	0.00220 ± 0.00008	0.00216
angles (deg)	0.401 ± 0.005	0.395
impropers (deg)	0.220 ± 0.005	0.221
quality of the structure		
% of residues in the most favorable region	88.2 ± 2.1	86.0
% residues in additional allowed regions	9.4 ± 3.0	12.8
% residues in generously allowed regions	2.5 ± 1.5	1.2
rmsd to the mean structure		
ordered backbone atoms (3.90)	0.71 ± 0.25 Å	0.62 Å
ordered heavy atoms (3.90)	1.11 ± 0.32 Å	0.99 Å
all backbone	0.92 ± 0.31 Å	0.93 Å
all heavy atoms	1.35 ± 0.38 Å	1.34 Å
equivalent X-ray resolution	1.6 Å	

[a] None of the 10 structures has a distance violation greater than 0.3 Å or a dihedral angle violation greater than 5°.

Location of the α-helical structure elements within the protein subunits have been unequivocally determined by the characteristic NOE patterns, ($i \rightarrow i + 3$) and ($i \rightarrow i + 4$), obtained from the 3D NOESY-HSQC spectra as well as by φ and ψ backbone torsion angles typical for the α-helical conformation. Identification of the α-helical elements is also supported by many medium- and long-range contacts. So, the four helices present in each of the subunits are the best defined regions in the whole protein structure (Table 4).

As in other S100 protein structures solved so far, the conformation of the linker between helices II and III and, in

Table 4: Rmsd Values of Secondary Structure Elements in 10 NMR-Derived Structures of *apo*-S100A1-βME Protein with the Lowest Total Energy

residues	structure elements	backbone atoms (Å)	all heavy atoms (Å)
3−17	helix I	0.23 ± 0.10	0.50 ± 0.15
30−40	helix II	0.14 ± 0.06	0.72 ± 0.23
52−63	helix III	0.19 ± 0.07	0.64 ± 0.20
72−89	helix IV	0.40 ± 0.17	0.81 ± 0.26

particular, the conformations of the Ca^{2+}-binding loops can be determined much less precisely because of few long-range contacts observed for these protein segments. Nevertheless, from the NOE spectra, and from the values of backbone torsion angles, it is evident that residues Lys 27, Leu 28, and Ser 29 in the N-loop and Glu 68, Val 69, and Asp 70 in the C-loop form an antiparallel β-sheet stabilized by a pair of hydrogen bonds between the amide and carbonyl groups of Leu 28 and Val 69. Analogous structures (*44*), common for EF-hand proteins, have been found in all S100 proteins studied so far.

The three-dimensional structure of the protein can be characterized as an "X-type" bundle with a large intersubunit interface formed by two pairs of antiparallel helices I, I′ and IV, IV′, similarly as in other S100 proteins (Figure 3).

Protons of residues situated at the subunit interface display numerous intersubunit NOEs. For example, protons in residues of helix I (Leu 4, Met 8, Leu 11, Ile 12, Val 14) give many contacts to protons in corresponding residues of helix I′ and protons in helix IV (Val 75, Val 76, Val 78, Ala 79, Thr 82) give contacts to residues of helix IV′. A number of cross-peaks have been assigned as arising from contacts between residues located at the N-terminus of helix I and the C-terminus of helix II′. For instance, H^{ϵ} protons of Met 8 in helix I give cross-peaks with protons situated not only in helix IV′ (H^{δ} of Leu 81 and H^{γ} of Val 78) but also in the C-terminus of helix II′ (H^{δ} of Leu 37) and in the hinge region (H^{δ} of Leu 41 and H^{ϵ} of Phe 44).

Chemical Shift Changes Induced by βME Modification. It is well-known that chemical shifts depend on local protein structure (*38*, *45*, *46*). Therefore, chemical shift differences between S100A1 and S100A1-βME molecules can be treated as indicators of these regions of the protein structure that are the most affected by the Cys 85 modification. It has been shown (*47*) that a weighted combination of H_N, C′, N, and C_α chemical shift differences, $\Delta\delta_{tot}$, is a very effective measure of structural changes in proteins. $\Delta\delta_{tot}$ values for the S100A1/S100A1-βME pair calculated using eq 1 given in ref (*47*) are shown in Figure 4. There are three parts of the protein where they substantially exceed the measurement error limits: Met 8 to Lys 25 segment comprising a large part of helix I and the N-terminal half of the N-loop, Glu 40 to Val 54 segment comprising the linker and the N-terminus of helix III, and Val 83 to Trp 90 segment of helix IV in the vicinity of the modification site (Cys 85). These data can be correlated with global conformational changes induced by the protein modification presented in Figure 5.

Rotational Diffusion. R_1, R_2 and NOE data have been obtained for all backbone amide nitrogen nuclei of *apo*-S100A1-βME protein at 11.7 T and for 86 ones at 9.4 T. For *apo*-S100A1 the relaxation data for only 72 out of 92 backbone amide nitrogen nuclei have been determined at 11.7 T and 67 ones at 9.4 T due to strong overlap of many resonances in the $^1H/^{15}N$ correlation spectrum, predominantly coming from amino acid residues located within helix I, the N-loop, and the C-terminus (see Supporting Information).

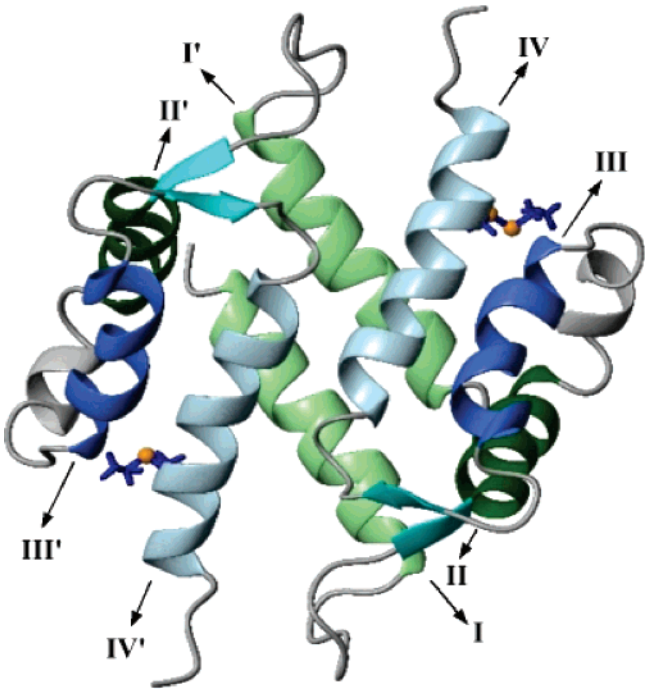

FIGURE 3: Ribbon drawing of the three-dimensional structure of *apo*-S100A1-βME protein. In both subunits the consecutive helices are labeled with Roman numbers and indicated by different colors. Helices I, I′, IV, and IV′, forming the intersubunit interface, are shown in light colors. The structure is oriented in the same way as those presented in Figures 2 and 5.

Ratios of principal values of moments of inertia can be used to calculate the predicted ratios of diffusion coefficients $D_\parallel/D_\perp$ (*48*). For S100A1-βME and S100A1 these ratios equal to 0.950 and 0.965, respectively (see Table 2). This prediction was confirmed by the analysis of experimental data using the anisotropic diffusion model. Experimentally determined diffusion coefficients yield $D_\parallel/D_\perp$ ratios very close to the predicted ones (see Table 2). Overall tumbling of both proteins is slightly anisotropic and well represented by the oblate tensors. The averaged isotropic rotational correlation times, τ_R, are typical for proteins of this size and correspond well to the result obtained for an another protein from the S100 family, i.e., S100B: 7.87 ns (*49*).

Protein Backbone Dynamics. There is no significant differentiation between local dynamics of various structural elements of *apo*-S100A1. The α-helices as well as the calcium-binding loops and the linker segments display similar average values of S^2 parameter, which is a measure of fast local motions in the picosecond time scale (Table 5). On the other hand, local dynamics in *apo*-S100A1-βME is more differentiated. Although the dynamics of helices III and IV and of the β-sheet structure is not affected by the protein modification, the restriction of N−H vector motions in helices I and II as well as in the linker seems to increase slightly. The most pronounced effects concern both calcium-binding loops N and C which become the "hot spots" of the protein, displaying the greatest motional freedom of their N−H vectors (see Table 5 and Figure 6). Another hot point appears at the linker−helix III junction (Val 51, Asp 52, and Ala 53).

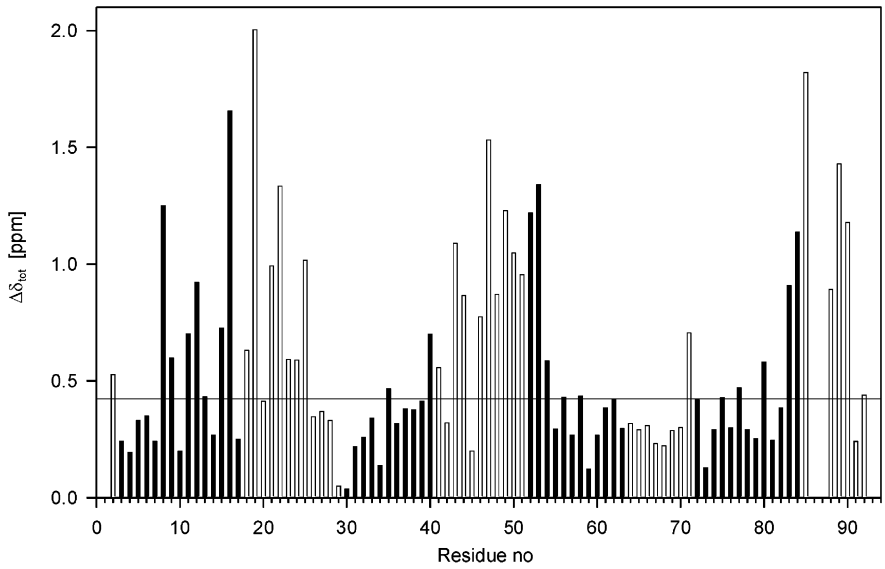

FIGURE 4: The combined chemical shift difference $\Delta\delta_{tot}$ between *apo*-S100A1 (unpublished results) and *apo*-S100A1-βME (BMRB database, acc. no. 4982) calculated according to eq 1 of ref 47. Average value of $\Delta\delta_{tot}$ is equal to 0.575, and its standard deviation (0.423) is marked by the horizontal black line. Black bars correspond to those residues that are in the α-helical conformation in both *apo*-S100A1 and *apo*-S100A-βME. $\Delta\delta_{tot}$ values for residues 86 and 87 are missing because chemical shifts for C′ of Asn 86 and for H_N and backbone N of Asn 87 could not be determined in *apo*-S100A1.

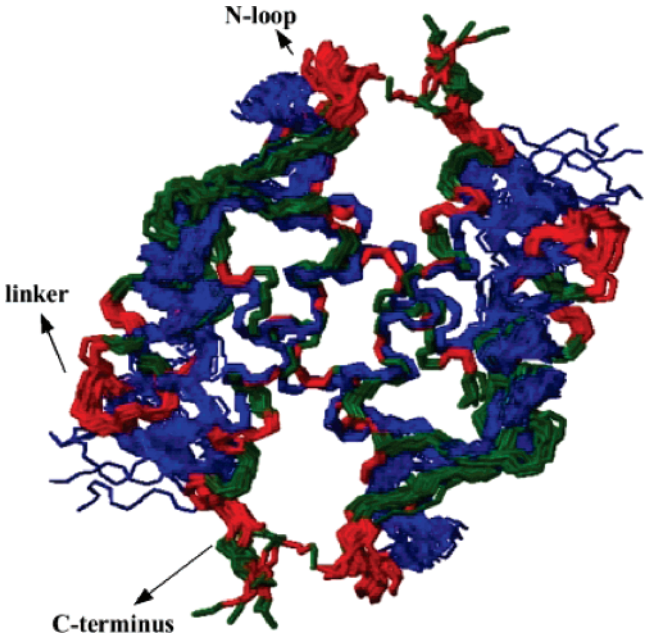

FIGURE 5: Overlay of ensembles of NMR structures of *apo*-S100A1 (blue) taken from the Protein Data Bank (accession code no. 1K2H) and of *apo*-S100A1-βME determined in this work (PDB accession code no. 2JPT). In the *apo*-S100A1-βME structures the residues for which $\Delta\delta_{tot}$ exceeds 0.423 are marked in red and all others in green, including two residues at the C-terminus: Asn 86 and Asn 87 for which the $\Delta\delta_{tot}$ values have not been measured (please compare with Figure 4). The structures are oriented in the same way as those presented in Figures 2 and 3.

For a few residues in the N-loop of *apo*-S100A1 (Ser 19, Glu 22, Lys 25), transverse relaxation rates R_2 are markedly greater than for any other residues (Table SI2) that indicates additional motions in the micro- to millisecond time scale affecting the transverse relaxation rates. Such processes referred to as chemical exchange effects can result in the nonzero R_{ex} term. A few residues in the N-loop of *apo*-S100A1-βME, similarly as in the unmodified protein, display large values of R_{ex} parameter (see Figure 7 and Table SI3).

Table 5: Weighted Mean Values of the Order Parameter S^2 of Structural Elements of Modified and Unmodified *apo*-S100A1 Protein[a]

structure element (a.a. residue)/no. of residues used in calcn	S100A1-βME	S100A1	ΔS^2
α-helix I (3−17)/11	0.95 (0.01)	0.88 (0.02)	+0.07 ± 0.02
α-helix II (30−40)/9	0.92 (0.01)	0.86 (0.02)	+0.06 ± 0.02
α-helix III (52−63)/11	0.94 (0.01)	0.93 (0.01)	
α-helix IV (72−84)[b]/12	0.95 (0.01)	0.93 (0.01)	
β-sheet (68−70)[c]/3	0.93 (0.02)	0.89 (0.02)	+0.04 ± 0.03
central part of N-loop (20−26)/6	0.79 (0.03)	0.86 (0.03)	−0.07 ± 0.04
central part of C-loop (64−67)/4	0.76 (0.03)	0.89 (0.02)	−0.13 ± 0.04
part of linker (41−50)/9	0.90 (0.01)	0.85 (0.01)	+0.05 ± 0.02
residues (3−89)/70	0.93 (0.01)	0.91 (0.01)	

[a] Standard deviations (in parentheses) and number of amino acid residues used in calculation are also given. Only these residues, for which data are available for both proteins, have been taken into consideration. [b] Helix IV in *apo*-S100A1-βME extends up to Phe 89, but only residues corresponding to helix IV in *apo*-S100A1 have been used in calculations. [c] Data are not available for residues Lys 27 to Ser 29 of *apo*-S100A1.

For two residues, Gly 23 and Lys 25, R_{ex} values at 9.4 T equal 3.6 ± 0.8 s^{-1} and 3.8 ± 0.4 s^{-1} in *apo*-S100A1-βME as compared with 1.1 ± 0.3 s^{-1} and 2.1 ± 0.5 s^{-1} in *apo*-S100A1, respectively. Most probably, insignificant R_{ex} value for Glu 22 in *apo*-S100A1-βME (0.4 ± 0.3 s^{-1}) in contrast to *apo*-S100A1 (4.5 ± 0.6 s^{-1}) is not due to the lack of an exchange process, but rather to a small chemical shift difference between exchanging conformations precluding manifestation of an exchange effect on the transverse relaxation rate. The R_{ex} difference for Glu 22 correlates with the largest backbone amide ^{15}N chemical shift difference of 7.2 ppm (122.5 and 115.3 ppm in *apo*-S100A1-βME and *apo*-S100A1, respectively) which can be only compared with the 7.0 ppm difference at the modification site (Cys 85). Different chemical exchange rates and/or different populations of the exchanging states in both

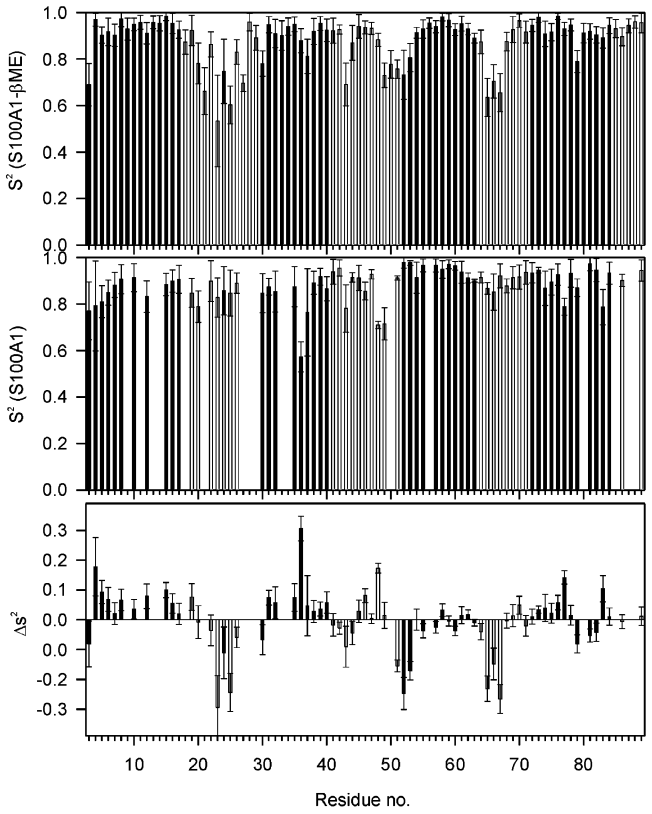

FIGURE 6: Order parameter values (S^2) with corresponding error bars as the function of amino acid sequence for *apo*-S100A1-βME (upper part) and *apo*-S100A1 (central part). In the lower part the differences $\Delta S^2 = S^2$(*apo*-S100A1-βME) $- S^2$(*apo*-S100A1) are shown. Black bars correspond to those residues that are in the α-helical conformation in both proteins. The data for the highly mobile terminal residues, Ser 2 and Trp 90 to Ser 93, are not shown since these residues cannot be regarded as a part of a rigid rotor.

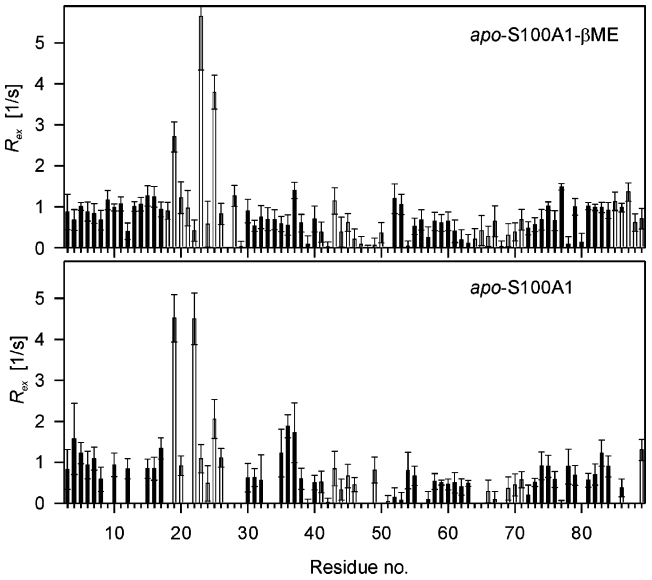

FIGURE 7: Chemical exchange terms (R_{ex}) at 9.4 T with corresponding error bars as a function of the amino acid sequence of *apo*-S100A1-βME (upper part) and *apo*-S100A1 (lower part). Black bars correspond to those residues that are in the α-helical conformation in both proteins. The data for the highly mobile terminal residues, Ser 2 and Trp 90 to Ser 93, are not shown since these residues cannot be regarded as a part of a rigid rotor.

proteins might be also responsible for the observed differences of R_{ex} values.

DISCUSSION

From the data presented in this paper the following picture of conformational changes induced in S100A1 protein by β-Me modification of Cys 85 can be derived:

(1) The primary effect of the modification is an elongation of helix IV. In *apo*-S100A1 (*4*) the last residue in the helical conformation is Ala 84, and the next, Cys 85, plays the role of the c-cap which NH group forms the hydrogen bond with the carbonyl of Leu 81 but which conformation ($\varphi = -136$, $\psi = +30°$) is drastically different from helical. In *apo*-S100A1-βME five other residues at the C-terminus assume the helical conformation documented by NOE contacts and $^3J(H_N,H_\alpha)$ scalar coupling constant measurements: Cys 85, Asn 86, Asn 87, Phe 88, and Phe 89. An analogous conformational transition at the C-terminus of helix IV of S100A1 protein arises from calcium coordination (*5*).

What mechanism is responsible for helix IV elongation in *apo*-S100A1-βME? Most probably it is a hydrophobic interaction between the βME moiety and the aromatic rings of Phe 88 and 89. From NOE measurements we could not obtain direct evidence for these contacts because β-mercaptoethanol used by us was not labeled with ^{13}C. Nevertheless, in the low-energy structures of S100A1-βME determined by us the distances between C_α of βME (HO$-C_\alpha H_2-C_\beta H_2 S-$) from $H_\epsilon 2$ and H_ζ protons of the Phe 89 ring equal merely 4.3 and 4.8 Å, respectively.

In our previous paper (*6*) we suggested that thionylation of the cysteine residue situated at the 12th position from the C calcium binding loop (Cys 85 in S100A1) regulates, maybe, biological functions not only of S100A1 but also of its many homologues, because cysteine is strictly preserved at this particular position in 7 out of 13 S100A1-like proteins isolated from various species. Remarkably, in all of them (but not in other S100 proteins) the 16th position (analogous to Phe 89 in S100A1) is occupied by phenylalanine[2] and the 15th position either by phenylalanine or by tyrosine with only one exception of S100A11. It seems, therefore, that in all these proteins thionylation of the cysteine situated at the 12th position from the C calcium binding loop can induce the same effect of elongation of helix IV, as a consequence of hydrophobic interactions between a moiety of a small thiol molecule attached to the cysteine with aromatic side chains of residues situated at positions 15 and 16.

(2) The C-terminal segment of helix IV created by the Cys 85 modification, formed by residues 85−89, attracts the N loop of the other subunit of the protein and drastically changes its spatial orientation (see Figure 5). Consequently, the intrinsic conformation of the loop is also changed in a dramatic way. This transition cannot be precisely described because neither in *apo*-S100A1 (*5*) nor in *apo*-S100A1-βME (this paper) has the exact conformation of the N-loop been determined. Nevertheless, the most important data characterizing conformational features of the N-loop in both proteins are available, *viz.*, φ and ψ angles of Leu 28 and Glu 32 and $\chi 1$ angle of Glu 32 have been evaluated (see Table 6) and the values of S^2 and R_{ex} parameters have been measured for many residues forming the N-loop (Figures 6 and 7 and Table SI3).

[2] With the unique exception of chick S100A11 protein in which Leu was identified at this position although Phe is preserved in four other S100A11 proteins isolated from man, mouse, pig, and rabbit.

Table 6: Conformational Data Concerning the Structural Scaffold Formed by Leu 28 and Val 69 in S100A1 Protein and of Glu 32 and Glu 73 Residues Providing the Most Important Ligands of Calcium Ions Coordinated by Its N- and C-Loop, Respectively

conformation	Leu 28 φ/ψ	Glu 32 $\varphi/\psi/\chi1$	Val 69 φ/ψ	Glu 73 $\varphi/\psi/\chi1$
apo-S100A1 (PDB code 1K2H)	+82°/−176°	−74°/−56°/−57°	−140°/+143°	−81°/−37°/+74°
holo-S100A1 (PDB code 1ZFS)	−82°/+167°	−62°/−50°/+48°	−122°/+151°	−60°/−40°/+62°
apo-S100A1-bMe (PDB code 2JPT)	−133°/+121°	−50°/−57°/+35°	−138°/+139°	−48°/−23°/+48°

Table 7: Angles between Axes of Helices I, II, and IV[a] in *apo*-S100A1[b] and *apo*-S100A1-βME (This Work)[c]

helices	*apo*-S100A1	*apo*-S100A1-βME	Δ in *apo*-S100A1-βME	Δ in *holo*-S100A1
I → II	119 ± 3	113 ± 2	6 ± 5	12 ± 4
I → IV	105 ± 2	124 ± 2	19 ± 4	24 ± 4
II → IV	−46 ± 2	−43 ± 3	within error	17 ± 2
I → I′	−167 ± 2	−170 ± 3	within error	within error
IV → IV′	178 ± 2	143 ± 5	−35 ± 6	−24 ± 5

[a] Calculated using the Interhlx program (*52*). The sign convention as in ref (*53*). [b] The protein structure was taken from the Protein Data Bank (accession code no. 1K2H). [c] Δ: Respective changes of interhelical angles induced by the βME modification or calcium binding to S100A1 as reported in ref (*5*).

In *apo*-S100A1 the N-loop segment is quite rigid and by no means properly adjusted for coordination of the calcium ion. The conformations of Leu 28—the central residue of the loop—and of Glu 32 providing the most important, bidentate ligand of Ca^{2+} ion are drastically different from those in *holo*-S100A1 (see Table 6). Upon βME modification of the protein the values of φ and ψ angles of both these residues and of $\chi1$ angle of Glu 32 change dramatically and become much closer to those in *holo*-S100A1. It may be expected that such a conformational transition considerably increases the N-loop affinity of *apo*-S100A1 for calcium since the proper orientation of central residues of calcium binding loops and of the glutamate residues always present at their C-termini is believed to be of crucial importance for calcium coordination by all EF-hand proteins (*50*, *51*).

In S100A1-βME the precise adjustment of the N-loop conformation necessary for calcium binding is additionally facilitated by increased mobility of this protein segment not only in the picosecond time scale (compare the S^2 parameter values given in Table 5) but also in the micro- to millisecond time scale as evidenced by the increased R_{ex} values for Gly 23 and Lys 25 (see the section "Protein Backbone Dynamics").

(3) The enhancement of fast internal motions is observed also for a number of residues situated within the C-loop (Table 5) although its conformation does not change significantly upon βME modification (Table 6).

(4) In the modified protein the orientation of helix IV is shifted in such a way that the helices forming the interface between the protein subunits (I, I′, IV, and IV′) assume exactly the same relative orientation as in *holo*-S100A1 protein (compare interhelical angles I/I′, IV/IV′, and I/IV listed in Table 7).

CONCLUSIONS

Thionylation of Cys 85 residue of *apo*-S100A1 by β-mercaptoethanol modifies, in many respects, the protein structure. Although it still remains "closed", unable to bind target proteins, it becomes more similar to that of *holo* protein, which explains why the affinity of S100A1 for calcium increases upon the thionylation.

Nevertheless, on the basis of the results presented in this paper it is not possible to explain why the Ca^{2+}-binding constants to thionylated S100A1 increase in such a drastic way (1 order of magnitude to its C-loops and as much as 4 orders of magnitude to N-loops) and why it changes dramatically the mechanism of metal binding from noncooperative to strongly cooperative one (*6*).

This intriguing phenomenon can be elucidated by further systematic structural and dynamic studies of a series of properly chosen protein mutants. Such a method was previously applied, with great success, by Chazin and his co-workers to study the mechanism of calcium binding to calbindin D_{9k} (*54*−*56*).

ACKNOWLEDGMENT

The access to a high field (17.6 T) NMR spectrometer obtained in frame of Large Scale Facility (LSF) in the Institute of Molecular Biotechnology (Jena, Germany) is acknowledged.

SUPPORTING INFORMATION AVAILABLE

Two tables containing backbone amide ^{15}N relaxation rates and NOEs of *apo*-S100A1-βME and *apo*-S100A1 at two magnetic fields: 9.4 and 11.7 T. One table containing model-free approach parameters for individual amino acid residues of both proteins. This material is available free of charge via the Internet at http://pubs.acs.org.

REFERENCES

1. Donato, R. (2001) S100: A multigenic family of calcium-modulated proteins of the EF-hand type with intracellular and extracellular functional roles, *Int. J. Biochem. Cell Biol. 33*, 637−668.
2. Heizmann, C. W., Fritz, G., and Schafer, B. W. (2004) S100 proteins: Structure, functions and pathology, *Front. Biosci. 7*, d1356−d1368.
3. Moore, B. (1965) A soluble protein characteristic of the nervous system, *Biochem. Biophys. Res. Commun. 19*, 739−744.
4. Rustandi, R. R., Baldisseri, D. M., Inman, K. G., Nizner, P., Hamilton, S. M., Landar, A., Landar, A., Zimmer, D B., and Weber, D. J. (2002) Three-dimensional solution structure of the calcium-signaling protein *apo*-S100A1 as determined by NMR, *Biochemistry 41*, 788−796.
5. Wright, N. T., Varney, K. M., Ellis, K. C., Markowitz, J., Gitti, R. K., Zimmer, D. B., and Weber, D. J. (2005) The three-dimensional solution structure of Ca^{2+}-bound S100A1 as determined by NMR spectroscopy, *J. Mol. Biol. 353*, 410−426.
6. Goch, G., Vdovenko, S., Kozłowska, H., and Bierzyński, A. (2005) Affinity of S100A1 protein for calcium increases dramatically upon glutathionylation, *FEBS J. 272*, 2557−2565.
7. Berridge, M. J., Lipp, P., and Bootman, M. D. (2000) The versality and universality of calcium signaling, *Nat. Rev. Mol. Cell Biol. 1*, 11−21.
8. Bolewska, K., Kozłowska, H., Goch, G., Mikołajek, B., and Bierzyński, A. (1997) Molecular cloning and expression in *Escherichia coli* of a gene coding for bovine S100A1 protein

and its Glu32 → Gln and Glu73 → Gln mutants, *Acta Biochim. Polon. 44*, 275−284.
9. Isobe, T, and Okuyama, T. (1981) The amino-acid sequence of the a subunit in bovine brain S-100a protein, *Eur. J. Biochem. 116*, 79−86.
10. Baldisseri, D. M., Rustandi, R. R., Zhang, Z., Tang, C., Bair, C. L., Landar, A., Zimmer, D. B., and Weber, D. J. (1999) ^{1}H, ^{13}C and ^{15}N NMR sequence-specific resonance assignments for rat *apo*-S100A1(αα), *J. Biomol. NMR 14*, 91−92.
11. Marion, D., Ikura, M., Tschudin, R., and Bax, A. (1989) Rapid recording of 2D NMR spectra without phase cycling. Application to the study of hydrogen exchange in proteins, *J. Magn. Reson. 85*, 393−399.
12. Kay, L. E., Keifer, P., and Saarinen, T. (1992) Pure absorption gradient enhanced heteronuclear single quantum correlation spectroscopy with improved sensitivity, *J. Am. Chem. Soc. 114*, 10663−10665.
13. Wishart, D. S., Bigam, C. G., Yao, J., Abildgaad, F., Dyson, H. J., Oldfield, E., Markley, J. L., and Sykes, B. D. (1995) ^{1}H, ^{13}C, and ^{15}N chemical shifts referencing in biomolecular NMR, *J. Biomol. NMR 6*, 135−140.
14. Delaglio, F., Grzesiek, S., Vuister, G. W., Zhu, G., Pfeifer, J., and Bax, A. (1995) A multidimensional spectral processing system based on UNIX pipes, *J. Biomol. NMR 6*, 277−293.
15. Bartels, C., Xia, T., Billeter, M., Güntert, P., and Wüthrich, K. (1995) The program XEASY for computer-supported NMR spectral analysis of biological macromolecules, *J. Biomol. NMR 5*, 1−10.
16. Goddard, T. D., and Kneller, D. G. *SPARKY 3*, University of California, San Francisco.
17. Wittekind, M., and Mueller, L. (1993) HNCACB, a high-sensitivity 3D NMR experiments to correlate amide-proton and nitrogen resonances with the alpha- and beta-carbon resonances in proteins, *J. Magn. Reson. 101B*, 201−205.
18. Grzesiek, S., and Bax, A. (1992) Correlating backbone amide and side chain resonances in larger proteins by multiple relayed triple resonance NMR, *J. Am. Chem. Soc. 114*, 6291−6293.
19. Muhandiram, D. R., and Kay, L. E. (1994) Gradient-enhanced triple-resonance three-dimensional NMR experiments with improved sensitivity, *J. Magn. Reson. 103B*, 203−216.
20. Bax, A., and Ikura, M. (1991) An efficient 3D NMR technique for correlating the proton and ^{15}N backbone amide resonances with the α-carbon of the preceding residue in uniformly ^{15}N/^{13}C enriched proteins, *J. Biomol. NMR 1*, 99−104.
21. Ikura, M., Kay, L. E., and Bax, A. (1990) A novel approach for sequential assignments of ^{1}H, ^{13}C, and ^{15}N spectra for proteins: heteronuclear triple-resonance three-dimensional NMR spectroscopy. Application to calmodulin, *Biochemistry 29*, 4659−4667.
22. Löhr, F., and Rüterjans, H. (1995) A new triple-resonance experiment for the sequential assignment of backbone resonances in proteins, *J. Biomol. NMR 6*, 189−197.
23. Grzesiek, S., Anglister, J., and Bax, A. (1993) Correlation of backbone amide and aliphatic sidechain resonances in ^{13}C/^{15}N-enriched proteins by isotropic mixing of ^{13}C magnetization, *J. Magn. Reson. 101B*, 114−119.
24. Farrow, N. A., Muhamdiram, R., Singer, A. U., Paskal, S. M., Kay, C. M., Gish, G., Shoelton, S. E., Pawson, T., Forman-Kay, J. D., and Kay, L. E. (1994) Backbone dynamics of a free and a phosphopeptide-complexed *Src* homology 2 domain studied by ^{15}N NMR relaxation, *Biochemistry 33*, 5984−6003.
25. Kay, L. E., Nicholson, L. K., Delaglio, F., Bax, A., and Torchia, D. A. (1992) Pulse schemes for removal of the effects of cross-correlation between dipolar and chemical-shift anisotropy relaxation mechanisms on the measurement of heteronuclear T_1 and T_2 values in proteins, *J. Magn. Reson. 97*, 359−375.
26. Zhukov, I., and Ejchart, A. (1999) Factors improving the accuracy of determination of ^{15}N relaxation parameters in proteins, *Acta Biochim. Polon. 46*, 665−671.
27. Shaka, A. J., Baker, P. B., and Freeman, R. (1985) Computer-optimized decoupling scheme for wideband applications at low-level operation, *J. Magn. Reson. 64*, 547−552.
28. Wüthrich, K. (1986) *NMR of Proteins and Nucleic Acids*, John Wiley, New York.
29. Clore, G. M., Gronenborn, A. M., Nilges, M., and Ryan, C. A. (1987) Three-dimensional structure of potato carboxypeptidase inhibitor in solution. A study using nuclear magnetic resonance, distance geometry, and restrained molecular dynamics, *Biochemistry 26*, 8012−8013.
30. Nilges, M. (1993) A calculation strategy fir the structure determination of symmetric dimers by ^{1}H NMR, *Proteins: Struct., Funct., Genet. 17*, 297−309.
31. Cornilescu, G., Delaglio, F., and Bax, A. (1999) Protein backbone angle restraints from searching a database for chemical shift and sequence homology, *J. Biomol. NMR 13*, 289−302.
32. Güntert, P., Braun, W., and Wüthrich, K. (1991) Efficient computation of three-dimensional structures in solution from nuclear magnetic resonance data using the program Diana, Caliba, Habas and Glomsa, *J. Mol. Biol. 217*, 517−530.
33. Güntert, P., Mumenthaler, C., and Wüthrich, K. (1997) Torsion angle dynamics from NMR structure calculation with a new program Dyana, *J. Mol. Biol. 273*, 283−298.
34. Brünger, A. T. (1992) *X-PLOR Version 3.1. A system for X-ray crystallography and NMR*, Yale University, New Haven, CT.
35. Schwieters, C. D., Kuszewski, J. J., Tjandra, N., and Clore, G. M. (2003) The Xplor-NIH NMR molecular structure determination package, *J. Magn. Reson. 160*, 65−73.
36. Korzhnev, D. M., Billeter, M., Arseniev, A. S., and Orekhov, V. Y. (2001) NMR studies of brownian tumbling and internal motions in proteins, *Prog. Nucl. Magn. Reson. Spectrosc. 38*, 197−266.
37. Stone, M. J., Fairbrother, W. J., Palmer, A. G., III, Reizer, J., Saier, M. H., Jr., and Wright, P. E. (1992) Backbone dynamics of the *Bacillus subtilis* glucose permease IIA domain determined from ^{15}N NMR relaxation measurements, *Biochemistry 31*, 4394−4406.
38. Lipari, G., and Szabo, A. (1982) Model-free approach to the interpretation of nuclear magnetic resonance relaxation in macromolecules 1. Theory and range of validity. 2. Analysis of experimental results, *J. Am. Chem. Soc. 104*, 4546−4570.
39. Woessner, D. E. (1962) Nuclear spin relaxation in ellipsoid undergoing rotational Brownian motion, *J. Chem. Phys. 37*, 647−654.
40. Baber, J. L., Szabo, A., and Tjandra, N. (2001) Analysis of slow interdomain motion of macromolecules using NMR relaxation data, *J. Am. Chem. Soc. 123*, 3953−3959.
41. Alexandrescu, A. T., and Shortle, D. (1994) Backbone dynamics of a highly disordered 131 residue fragment of staphylococcal nuclease, *J. Mol. Biol. 242*, 527−546.
42. Brutscher, B., Brüschweiler, R., and Ernst, R. R. (1997) Backbone dynamics and structural characterization of the partially folded A state of ubiquitin by ^{1}H, ^{13}C, and ^{15}N nuclear magnetic resonance spectroscopy, *Biochemistry 36*, 13043−13053.
43. Laskowski, R., Rullmann, J., MacArthur, M., Kaptein, R., and Thornton, J. (1996) AQUA and PROCHECK-NMR: programs for checking the quality of protein structures solved by NMR, *J. Biomol. NMR 8*, 477−486.
44. Strynadka, N. C. J., and James, M. N. G. (1989) Crystal structures of the helix-loop-helix calcium-binding proteins, *Annu. Rev. Biochem. 58*, 951−998.
45. de Dios, A. C., and Oldfield, E. (1996) Chemical Shifts in Biochemical Systems, in *Encyclopedia of NMR* (Grant, D. M., and Harris, R. K., Eds.) Vol. 2, pp 1330−1336, John Wiley & Sons, Chichester.
46. Wishart, D. S., and Sykes, B. D. (1994) Chemical shifts as a tool for structure determination, *Methods Enzymol. 239*, 363−392.
47. Ayeda, A., Mulder, F. A. A., Yi, G.-S., Lu, Y., Kay, L. E., and Arrowsmith, C. H. (2001) Latent and active p53 are identical in conformation, *Nat. Struct. Biol. 8*, 756−760.
48. Mandel, A. M., Akke, M., and Palmer, A. G., III (1995) Backbone dynamics of *Escherichia coli* ribonuclease HI: correlation with structure and function in an active enzyme, *J. Mol. Biol. 246*, 144−163.
49. Inmam, K. G., Baldisseri, D. M., Miller, E, K., and Weber, D. J. (2001) Backbone dynamics of the calcium-signaling protein apo-S100B as determined by ^{15}N NMR relaxation, *Biochemistry 40*, 3439−3448.
50. Grabarek, Z. (2005) Structure of trapped intermediate of calmodulin: calcium regulation of EF-hand proteins from a new perspective. *J. Mol. Biol. 346*, 1351−1366.
51. Grabarek, Z. (2006) Structural basis for diversity of the EF-hand calcium-binding proteins. *J. Mol. Biol. 359*, 509−525.
52. Ikura, M. (1998) http://nmr.uhnres.utoronto.ca/ikura/interhlx/.

53. Drohat, A. C., Amburgey, J. C., Abilgaard, F., Starich, M. R., Baldisseri, D., and Weber, D. J. (1996) Solution structure of rat *apo*-S100B($\beta\beta$) as determined by NMR spectroscopy, *Biochemistry 35*, 11577−11588.
54. Bunick, C. G., Nelson, M. R., Mangahas, S., Hunter, M. J., Sheehan, J. H., Mizoue, L. S., Bunick, G. J., and Chazin, W. J. (2004) Designing sequence to control protein function in an EF-hand protein, *J. Am. Chem. Soc. 126*, 5990−5998.
55. Nelson, M. R., Thulin, E., Fagan, P. A., Forsen, S., and Chazin, W. J. (2002) The EF-hand domain: A globally cooperative structural unit, *Protein Sci. 11*, 198−205.
56. Mäler, L., Blankenship, J., Rance, M., and Chazin, W. J. (2000) Site−site communication in the EF-hand Ca^{2+}-binding protein calbindin D_{9k}, *Nat. Struct. Biol. 7*, 245−250.

BI701762V